Electrical Power and Energy Systems 158 (2024) 109939

Contents lists available at ScienceDirect

International Journal of Electrical Power and Energy Systems

journal homepage: www.elsevier.com/locate/ijepes

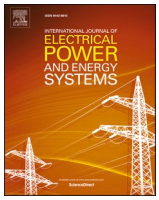

A consecutive power dispatch in wind farms to mitigate secondary frequency dips

Yi Cheng [a], Huadong Sun [a,*], Yuyuan Zhang [b], Shiyun Xu [a], Bing Zhao [a], Petr Vorobev [c], Vladimir Terzija [d]

[a] National Key Laboratory of Grid Security (China Electric Power Research Institute), Haidian District, Beijing 100192, China
[b] Beijing Electric Power Economic Technology Institute, Beijing, China
[c] Nanyang Technological University, Singapore, Singapore
[d] School of Engineering, Merz Court E4.41, Newcastle University, UK

ARTICLE INFO

Keywords:
Frequency nadir (FN)
Frequency support
Over-deceleration
Persistent energy reserves
Secondary frequency drip (SFD)
Temporary energy reserves

ABSTRACT

With the rapid increase of wind energy integrated into power systems, wind turbine generators (WTGs) are required to provide frequency support to maintain the system frequency stability. However, the frequency regulation is achieved by employing temporary energy reserves from WTGs at the initial stage of a disturbance. Therefore, a second frequency dip (SFD) may occur, if no other energy reserve is available to compensate the power deficiency as WTGs have to recover their operating points and rotor speeds back to the initial operating points. To deal with this problem, this paper proposes a consecutive power dispatch scheme to reduce the SFD and prevent WTGs from over-deceleration. All WTGs are divided into two groups with in a wind farm: Group 1 (G1) WTGs operating at maximum power point tracking (MPPT), Group 2 (G2) WTGs operating at deloading power. If a frequency contingency occurs, the proposed scheme aims to release an amount of kinetic energy (KE) stored in the rotating masses of G1 WTGs to improve the frequency nadir (FN). Following this, energy reserves are released from G2 WTGs to compensate the power shortage during the period when G1 WTGs rotor speeds have to be recovered. The simulation results show that the scheme causes a small SFD while improving the first FN and preventing the rotor from over-decelerations in various wind conditions, contingency sizes, and wind penetration levels.

1. Introduction

With the ongoing trend of reducing the reliance on fossil energy and the growing emphasis on improving the human living environment, renewable energy sources (RESs) have become mainstream in power systems. The International Renewable Energy Agency (IREA) predicts that wind power will account for 35 % of electricity demand and become the main power source by 2050 [1]. This will impose a double stress on the existing power systems: not only the wind energy sources bring natural intermittency, but also change the dynamic properties of the power system, in particular, its frequency behavior during major power imbalance events.

In conventional power systems, natural inertial response of synchronous generators (SGs) during power imbalance events contributes greatly to frequency stability within the first seconds after the disturbance. When a power disturbance occurs, SGs inherently release the kinetic energy (KE) stored in the rotating masses to support the system frequency before the frequency control system has time to react. However, the increase of penetration level of variable speed wind turbine generators (WTGs), i.e., doubly-fed induction generator (DFIG) and fully rated converter generator (FRCG), dramatically decreases the inertial capabilities, making frequency less stable during the first moments after a disturbance [2]. Since WTGs are connected to the power system through power converters, their rotors are not directly coupled to the power system frequency, thus they do not provide natural inertial response during frequency disturbance events. As a result, for power systems with high penetration level of RESs, frequency nadirs (FNs) are more likely to fall into the impermissible frequency range following contingencies. To cope with this problem, the system operators in some countries require provision of specially designed inertial response from large-scale wind farms (WFs) [3,4].

Among all the latest literature sources, schemes attempting to release frequency control through WTGs participation can be divided into two categories: (1) temporary energy-based inertial control and (2) persistent energy-based deloading control. Some researchers propose to

* Corresponding author.

https://doi.org/10.1016/j.ijepes.2024.109939
Received 21 August 2023; Received in revised form 20 December 2023; Accepted 11 March 2024
Available online 17 March 2024

Nomenclature

Abbreviations

AGC	Automatic generation control
ASGs	Asynchronous generators
DFIG	Doubly-fed induction generator
FN	Frequency nadir
FRCG	Fully rated converter generator
KE	Kinetic energy
MPPT	Maximum power point tracking
RESs	Renewable energy sources
SGs	Synchronous generators
SFD	Second frequency dip
TSR	Tip-speed ratio
WFs	Wind farms
WTGs	Wind turbine generators

operate WTGs slightly away from MPPT curve to have excess wind power available for possible contingency. This can be achieved by either rotor speed control [5,6] or pitch angle control [5,7,8] respectively. Although it ensures that WTGs will be able to contribute effectively to frequency support, it also reduces the annual revenues due to WTGs not working at MPPT. Additionally, there is an adverse impact on the lifetime of WTGs due to excessive fatigue, as frequent changes of pitch angle are inevitable in this case.

Another category of frequency response schemes from WTGs is corresponds to mimicking the inertial response of SGs, which enables WTGs to operate according to MPPT and temporarily utilise the KE stored in the rotating masses of the turbines to stop the frequency decline [9–13]. To minimize the adverse impact brought by the conventional virtual inertial control, reference [12] proposes an improved control that suggests various operating power tracking methods. The rotor speed recovery strategy based on variable-coefficient PI control is proposed to minimize the secondary frequency dip (SFD). Reference [14] proposes a control method to avoid second frequency dips caused by virtual inertial response. The main idea of this control is to maintain the continuity and smoothness of the output power when the virtual inertial response is withdrawn. Unlike traditional strategies that directly switch to MPPT mode following the conclusion of the inertial response phase, this method gradually adjusts the output power of the DFIG to avoid a sharp decrease in the provided power. The effectiveness of this strategy in improving frequency response has been verified by simulations. Reference [15] proposed a scheme that progressively reduces power reference during the WTG rotor speed recovery stage, which results in a lighter SFD and a shorter speed recovery time. In [16], an even smoother WTG rotor speed restoration strategy is proposed in order to reduce the rapid power decrease so that the size of the SFD is reduced. In reference [17], the mitigation of the secondary frequency dip is achieved by regulating the number of generator units involved in frequency support, strategically withdrawing their participation at distinct moments of time. This approach aims to replace the otherwise abrupt transition to normal operating mode with a more gradual shift from the emergency to normal conditions. A similar scheme concept is presented in reference [18], which revolves around solving an optimal control problem to minimize overall energy losses. In reference [19], the sharp decline in active power provision following the conclusion of the over-production period is replaced by a gradual reduction linked to four specific parameters. The values of these parameter are dynamically updated according to a specific look-up table.

In this context, the core problem in applying virtual inertia-type control is that after the frequency support period concludes or when the minimum WTG rotor speed protection system is triggered, rotor speed must recover back to its optimum value. Consequently, an SFD appears due to a sudden loss of power response from WTGs. In the system with high penetration level of wind power sources, the more wind power is delivered to the grid, the more severe the SFD is and its amplitude can even become larger than the amplitude of the first FN. Previous research has made noteworthy progress in augmenting the frequency support capabilities of Wind Turbine Generators (WTGs) and mitigating adverse effects resulting from the cessation of their frequency support due to insufficient stored energy. However, persistent challenges such as poor efficiency, unexpected performance, and even high costs continue to affect aforementioned methodologies.

This paper introduces a novel scheme for the frequency support from WTGs that allows to reduce the secondary frequency dip. For this, all WTGs in every wind farm are supposed to be divided into two groups. Group 1 (G1) includes WTGs operating according to MPPT, while the Group 2 (G2) represents WTGs operating in a deloaded mode. G1 WTGs with dynamic droop-based control release the temporary energy to support frequency until all the available kinetic energy is used up. Following that, G2 WTGs take over the duty of frequency response by decreasing their rotor speeds, thus smoothly releasing the additional energy to compensate the power deficiency caused by the withdrawal of the virtual inertia response from the Group 1. This scheme employs two distinct controller algorithms for G1 and G2 WTGs respectively, aiming to coordinated release of kinetic energy during the frequency response time. Case studies under varied operating conditions, disturbances sizes, and wind penetration levels are conducted to demonstrate the effectiveness of the proposed approach to provide frequency support and prevent the premature withdrawal of the response during the critical phase of the transient. Consequently, the issue of SFD is effectively addressed. In summary, the key contributions of this study can be outlined as follows:

- A frequency support methodology has been proposed, incorporating dynamic-droop control from WTGs, to utilize their kinetic energy to provide enhanced system frequency control.
- A consecutive power dispatch scheme was proposed to effectively coordinate the responses from different WTGs, with the primary aim of mitigating secondary frequency dips.
- To evaluate the efficiency of the proposed method, three simulation scenarios are applied and performed in test power system using DIgSILENT PowerFactory software. Results confirm the effectiveness of the proposed scheme.

The paper is organized as follows. In Section 2, DFIG-based wind energy conversion system is presented. In Section 3, the consecutive power dispatch scheme is proposed. Section 4 introduces the system model used for simulating all the test cases. In Section 5, case studies are carried out to demonstrate the performance of proposed scheme under different wind speeds, disturbance sizes and wind power penetration levels. Section 6 concludes the paper.

2. DFIG-based wind energy conversion system

2.1. DFIG model

A DFIG-based wind energy conversion system is chosen in this paper, and a typical configuration of DFIGs is shown in Fig. 1. It is composed of rotating part, gearbox, induction generator and two back-to-back PWM voltage source converters rated at about 30 % of nominal generator power. The speed range of this type of turbine is ±30% around the synchronous speed [20] which generally is 0.7 pu. to 1.25 pu.[21,22]. For the purposes of this paper, it is justified to use a single-mass model for the mechanical dynamics of WTGs [23]. It is represented by the following equation:

$$2H_{DFIG}\omega_r\frac{d\omega_r}{dt} = P_m - P_e \tag{1}$$

where H_{DFIG} represents inertia constant of the turbine of DFIG, ω_r rep-

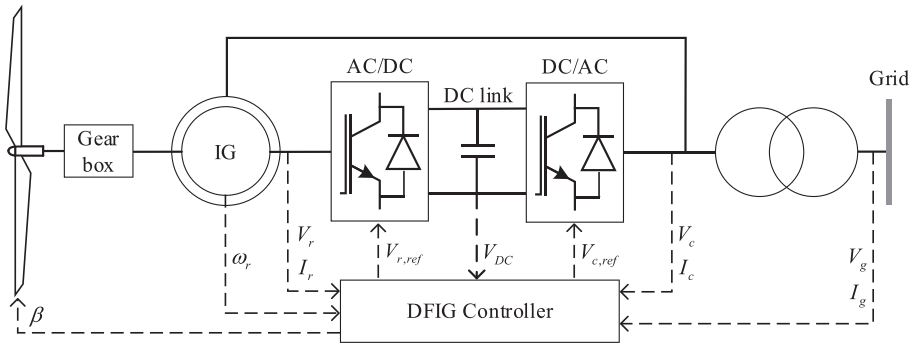

Fig. 1. Typical configuration of a DFIG.

resents the rotor speed, P_m and P_e represents mechanical power and electrical output power, respectively.

2.2. Aerodynamic system

According to the aerodynamic theory, the mechanical power P_m extracted from wind at any given wind speed is defined as

$$P_m = \frac{1}{2}\rho A v_w^3 C_p(\lambda,\beta) \tag{2}$$

where ρ is the air density in kg/m^3, A is the blade-swept area in m^2, v_w is the wind speed in m/s, $C_p(\lambda,\beta)$ is the power coefficient, which is dependent on λ - the tip-speed ratio (TSR), $\lambda = \omega_r R/v_w$, β- the pitch angle and ω_r- the rotor speed. $C_p(\lambda,\beta)$ is dependent on the aerodynamic design [24] and is specified by the turbine manufactures [25]. This nonlinear relationship between C_p and λ can be described as

$$C_p(\lambda,\beta) = 0.22(116\lambda_i - 0.4\beta - 5)e^{-12.5\lambda_i} \tag{3}$$

$$\lambda_i = \frac{1}{\lambda + 0.08\beta} - \frac{0.035}{\beta^3 + 1} \tag{4}$$

Fig. 2 shows the power-wind speed curve of a DFIG used in this paper. The blue curve is divided into four regions depending on the wind speed value. The cut-in, rated and cut-out speeds of the DFIG in question are 4 m/s, 11 m/s, and 25 m/s, respectively. In addition, power captured by WTGs is limited by the level of nominal power to mitigate the mechanical stress on WTGs. However, under extreme weather conditions, i.e., wind speed is larger than the cut out speed, WTGs have to terminate their operations to prevent further damages.

2.3. Maximum power point tracking (MPPT)

The MPPT control enables WTGs to convert as the maximum possible wind energy to electric energy at various wind speeds. Fig. 3 represents

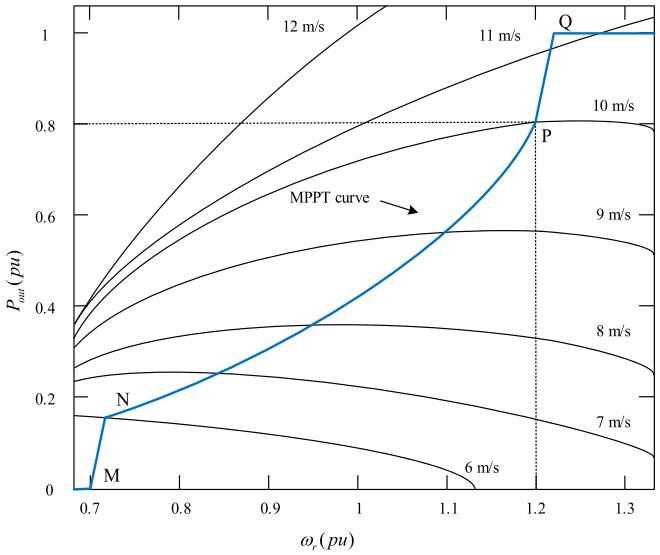

Fig. 3. Active power-rotor speed curve of a DFIG for different wind speeds [19].

the active power- rotor speed curve of a DFIG for each wind speed. The MPPT curve, i.e., the blue line, can be separated into four operation regions. The first region (M−N) represents the condition in which the active power contributed from the WTGs approximately follows a linear trend. Then, the WTG moves to its MPPT mode (N-P) and contributes maximum power available to the grid. In the third region (P-Q), the WTG operates at a constant rotor speed which avoids the overspeeding. In case the instant wind speed exceeds the rated value (Q), constant power mode is switched in to assure a rated output power.

To generate the maximum wind energy, the reference for MPPT

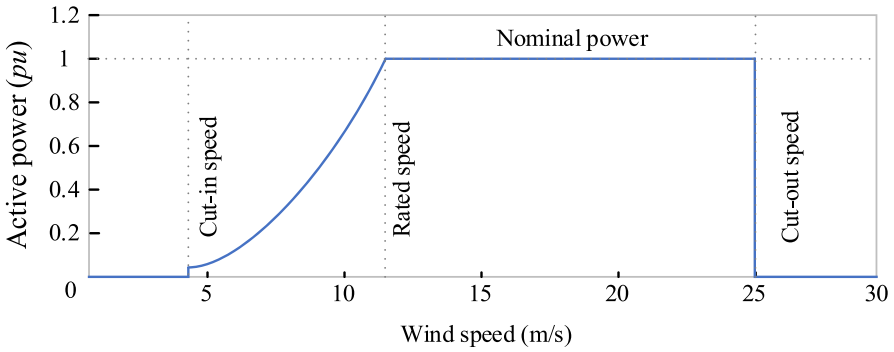

Fig. 2. Power-wind speed curve of a DFIG [26].

control, P_{MPPT}, is expressed as

$$P_{MPPT} = k_{opt}\omega_r^3 \tag{5}$$

$$k_{opt} = \frac{1}{2}\rho\pi\frac{C_{p,\max}}{\lambda_{opt}^3}R^5 \tag{6}$$

where k_{opt}, $C_{p,\max}$ and λ_{opt} are MPPT coefficient, maximum power coefficient and optimum TSR, respectively. In this paper, the pitch angle is assumed to be constant ($\beta = 0^{\circ}$), hence pitch angle control is not active. Therefore, C_p is solely determined by λ. The $C_{p,\max}$ is set to 0.4382 and λ_{opt} is set to 6.309.

2.4. Dynamic droop-based inertial control [10]

This subsection explains the characteristics of the dynamic droop-based scheme described in [10] which improves the FN during the transient In order to overcome the shortage of fixed-gain inertial control discussed in [27] the droop loop only contributes during the initial stage of a contingency and large gain used may cause the over-deceleration of the rotor, dynamic droop $R(df/dt)$ is dynamically changing depending on the RoCoF in [10]. During the very first instants of a frequency contingency, $R(df/dt)$ is turned to be a relatively small value due to a large RoCoF occurs at this stage, which enables DFIGs to release large amount of ΔP supporting frequency. To prevent the rotor from a result of over-deceleration, $R(df/dt)$ increases with change of RoCoF which make ΔP decrease. In addition, the reduction in ΔP can also mitigate the amplitude of SFD due to the termination of the temporal energy support where minimum rotor speed is reached.

The inertial control loop for the dynamic-droop based scheme is shown in Fig. 4. The reference power point P_{ref} consists of P_{MPPT} and output of the droop loop ΔP.

In this scheme, ΔP is expressed as

$$\Delta P = -\frac{1}{R(df/dt)}(f_{mea} - f_{nom}) \tag{7}$$

where $R(df/dt)$ represents the dynamic droop.

2.5. Deloading operation of DFIGs

In order for DFIGs to have sufficient active power to provide frequency support two main deloading methods, pitch angle control and rotor speed control, are widely implemented in WTGs. Pitch angle control changes the pitch angle of the blades, which deloads the WTG related to a possible maximum power point at the given wind speed. As can be seen from (2) to (4), as β becomes larger, it reduces C_P, thereby also reducing P_m. However, rotor speed control is utilized in this paper because the pitch angle control requires frequent change of pitch angle, which may affect the lifetime of the pitch controller and may increase maintenance costs [6]. Regarding the rotor speed control, WTGs can be deloaded by shifting the operating point towards left (point B) or right (point C) from the MPPT point, hence known as underspeeding or overspeeding control, respectively in Fig. 5. In this paper, the deloading operation is accomplished by overspeeding control, because an underspeeding controlled turbine can be deteriorating to the system stability [28]. For example, rotor speed increases from $\omega_{\max}$ to ω_{de} when WTG deloads from maximum power $P_{\max}$ to deloaded power P_{de}. When there is a frequency drop the KE stored in the rotating mass is released as the rotor speed decreases. Most of WTGs are deloaded between 10 % and 20 % depending on the instantaneous wind speed and given rotor speed limit [6].

A deloading coefficient $d = 10\%$ is employed, then deloaded power can be expressed by

$$P_{de} = 0.9P_{MPPT} \tag{8}$$

$$P_{de} = \frac{1}{2}\frac{\rho AR^3(1-d)C_{p\_\max}\omega^3}{\lambda_d^3} \tag{9}$$

Since, $C_{p\_de} = (1-d)C_{p\_\max}$,

$$P_{de} = (1-d)P_{mppt} = \frac{1}{2}\rho\pi R^2 C_{p,de}v^3 \tag{10}$$

where $C_{P,de}$ is the deloading power coefficient.

3. Description of consecutive power dispatch method

The traditional frequency control schemes for conventional power plants offer an extensive and flexible range of solutions for systems operators, especially during system faults and unexpected disturbances. For example, controlling the position of the main supply valve in case of a steam generator can effectively compensate the active power imbalance, while it is impossible to instantaneously control WTGs, or even to

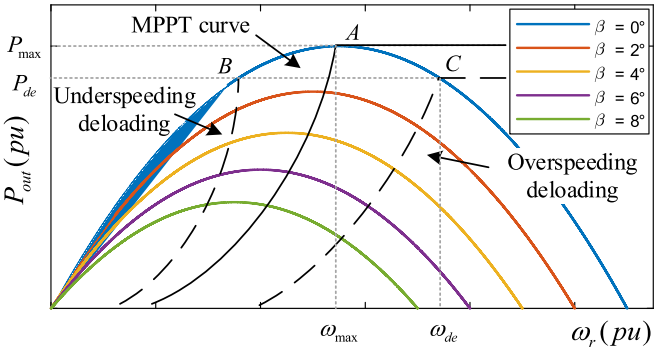

Fig. 5. MPPT and deloading power curve of DFIG.

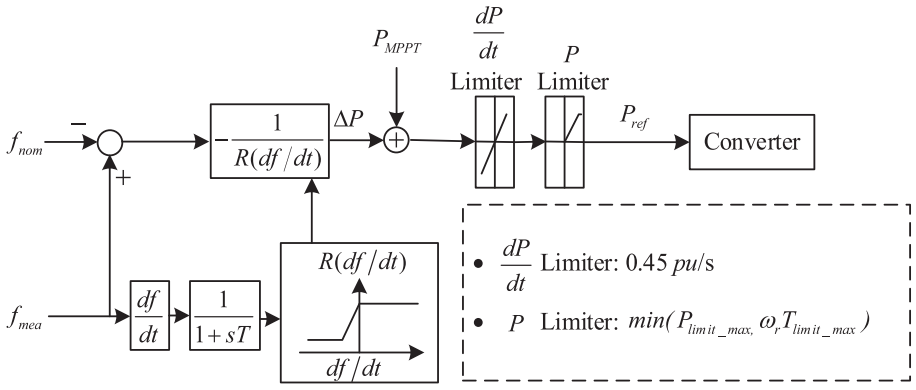

Fig. 4. Inertial control loop for the dynamic droop-based scheme.

have an accurate prediction of their output due to the intermittence of wind speed. To balance this highly non-dispatchable resource, other generation units have to be regulated more frequently. Therefore, WFs are desperately subjected to have similar performance to conventional generations so that demand given by system operators can be met.

3.1. Explanation of temporary and persistent energy reserves

The energy reserves supplied by WF for frequency regulation can be classified into two categories: temporary and persistent energy reserves.

The temporary energy reserves correspond to the energy, stored as the rotor kinetic energy of the WTGs operating at the MPPT curve, which contributes to the FN and RoCoF at the very first instants of a frequency disturbance. The duration of the temporary energy reserves depends on the time that the rotor speed of WTGs decreases from its nominal speed to minimum speed (0.7 *pu*). On the other hand, the persistent energy reserves correspond to the WTGs being operated away from their MPPT curve – i.e., at a suboptimal power level, which makes them able to provide frequency support for extended period of time. It is worth noting that if frequency support is not required from the Wind Turbine Generators (WTGs) that operate in suboptimal mode, those WTGs still deliver active power at a suboptimal level to the grid.

Dispatching the temporary and persistent energy reserves in a WF is a key problem to mitigate the impacts caused by a possible occurrence of an SFD. In this process, the WTGs operating at the optimal point are designed to employ a dynamic droop-based control to provide initial active power response. However, the persistent energy reserves stored in the WTGs operating at the suboptimal point are planned to compensate the power shortage caused by the withdrawal of the initial frequency response. Fig. 6 depicts the consecutive dispatch of temporary and persistent energy reserves for arresting the SFD. The Area 1 and Area 2 represent the temporary reserve power and the active power shortage due to the restoration of the rotor speed, respectively. In case a system disturbance occurs at t_{dis}, WTGs operating at the optimal point initially provide a temporary power P_{droop}, which typically lasts up to about ten seconds and the termination time t_{ter} is determined by when the moment the rotor speed of WTGs reaches to the minimum value of 0.7 pu. The larger the P_{droop} is, the faster the active power imbalance can be compensated, which brings a severer SFD. Therefore, adaptive strategies for releasing P_{droop} are discussed in the next section. During the restoration period (between t_{ter} and t_{re}) of the rotor speed, the persistent energy reserves, marked as Area 3, are released in order to counterbalance the power reduction ΔP_{re}. Thus, the difference between Area 2 and Area 3 determines the magnitude of the SFD. In order to make sure the annual revenues of WFs are maximized, the number of WTGs operating at suboptimal point needs to adapt to the disturbance event size. For instance, if the amount of persistent energy reserves is smaller than that of the corresponding power reduction, an appearance of an SFD is unavoidable, which may cause a likelihood of lower FN comparing to the first swing.

3.2. Consecutive dispatch of temporary and persistent energy reserves

The trade-off between fast inertial response and rotational speed recovery is the vital issue to be settled. To suppress the SFD and make the most use of frequency support capability of WTGs, an application of employing persistent energy reserves is to deliver additional active power during the rotor restoration stage.

This paper proposes a modified power dispatch for DFIG-based WFs, which handles aforementioned problems in a leader–follower manner. To achieve this, all WTGs in a WF are divided into two groups depending on the operational conditions. The first group (G1) includes WTGs operating at MPPT with a dynamic droop control, while the second group (G2) contains WTGs operating at suboptimal mode realized by overspeeding control. In the normal operating condition, all WTGs feed active power to the grid depending on predefined operating point. When a frequency disturbance occurs in the power system, G1 attains fast frequency regulation and terminates the support at the time instant when rotor speed of G1 WTGs reduces to 0.7 *pu*. Then a trip signal which triggers the release of the persistent reserves is sent to G2 thus arresting a sequential frequency dip caused by the withdrawal of temporary frequency support by G1. We note, that the loss in annual revenue from such a multi-operation mode of WF is less compared to a WF consisting of all deloaded WTGs. However, communication of each WTG is required with a central WF controller. A latency time of 200 ms [29] between action of two frequency support modes from two groups of WTGs is caused by communication networks and computation time. Fig. 7 shows the schematic of implementing WTGs in the proposed frequency control scheme.

4. System model

Fig. 8 demonstrates a system model built in DIgSILENT PowerFactory software package to validate the performance of the consecutive dispatch of temporary and persistent energy reserves. A system model consists of four SGs, one aggregated DFIG-based WF, and a general load of 300 MW.

4.1. Synchronous generators

Four SGs are present in the system: three 300 MVA SGs and one 200 MVA SG. All SGs in this paper are considered to be powered by steam turbines. Fig. 9 shows the IEEE Type-1 speed-governor model. The inertia time constants of all SGs are set to 6.25 s. SG1 is selected as a slack machine and SG2 is used to simulate a frequency contingency by disconnecting it from the rest of the system at a certain time moment.

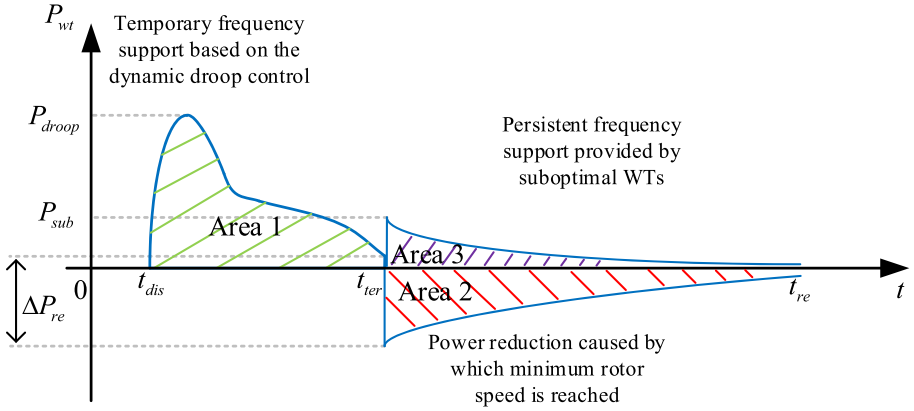

Fig. 6. Consecutive dispatch of temporary and persistent energy reserves provided by WTGs operating at optimal point and suboptimal point, respectively.

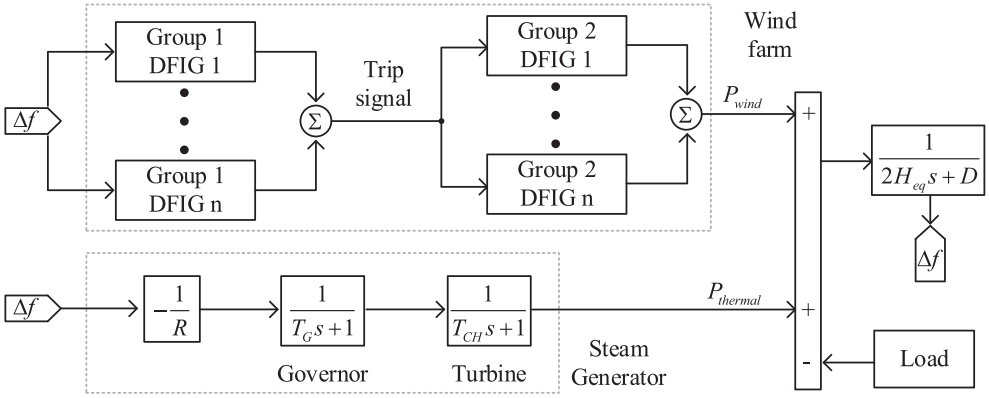

Fig. 7. Block diagram of implementing WTGs in frequency control.

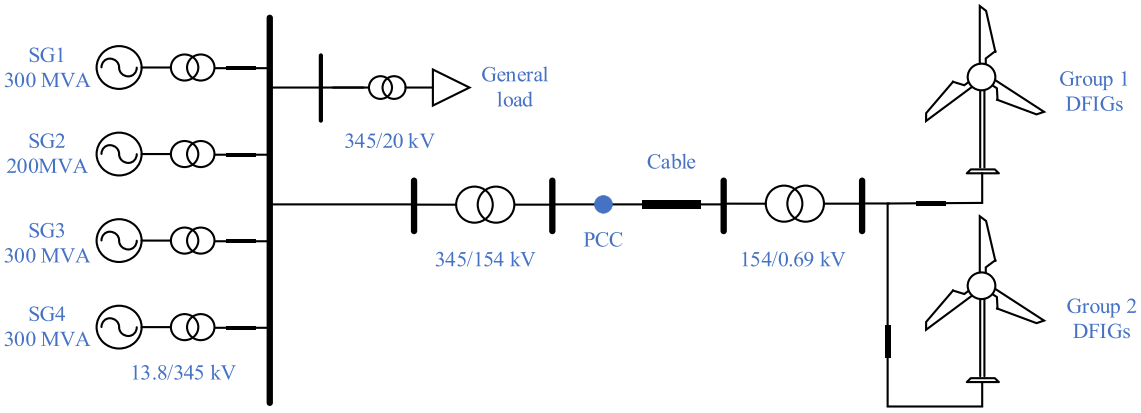

Fig. 8. System model.

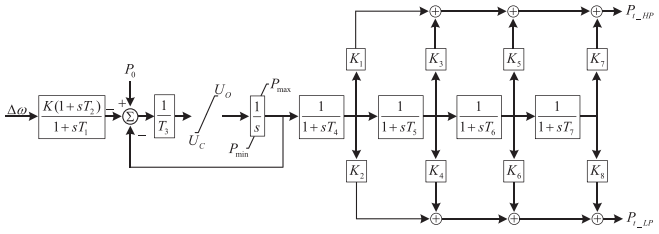

Fig. 9. IEEE Type 1 speed-governor in PowerFactory.

Since the automatic generation control (AGC) is not modeled in our setup, the frequency does not get completely recovered to the nominal value after the contingency.

4.2. DFIG-based WF

The DFIG-based WF is connected to the 0.69/154 kV transformer through the 154 kV submarine cable, then connected to the grid. This WF is divided into two groups of WTGs with 70 % of DFIGs operating at MPPT curve and 30 % of DFIGs operation in deloaded mode as specified above. The rated power of each DFIG is 2 MW.

In this study, we model the DFIG-based WF in PowerFactory software, the block diagram of proposed scheme for is shown in Fig. 10. The

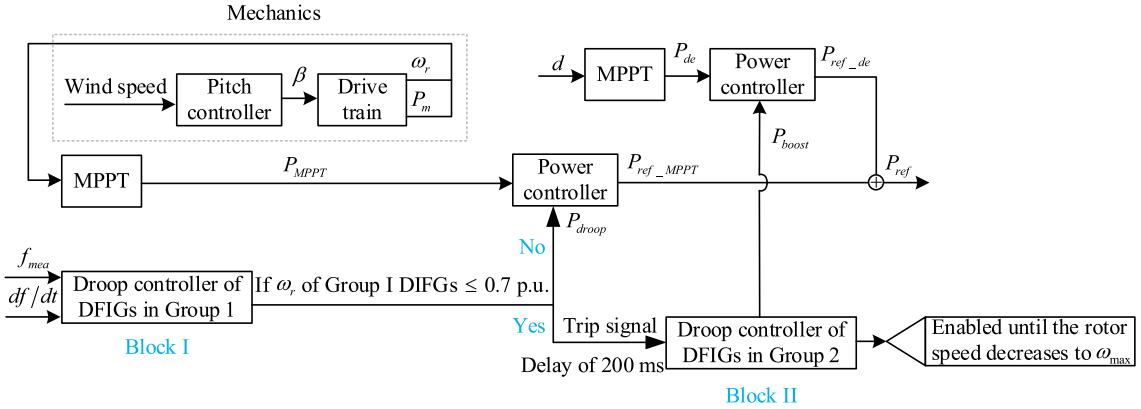

Fig. 10. Block diagram of the proposed scheme for DFIG-based WF in DIgSILENT PowerFactory.

mechanics part of DFIG consists of a pitch angle controller and a drive train. The pitch angle controller sends the constant pitch angle signal to the drive train. The Drive train uses Equations (2)-(4) to model aerodynamics of the DFIG using a single-mass representative. The electromechanical transient dynamics of the drive train is not considered in this paper. The MPPT calculates the optimum wind power and the power controller modulates the active power of the WF. On the other hand, a deloading factor is sent to MPPT block in G2 DFIGs, which is used to make G2 DFIGs operate at a deloaded level. The Block I shown in Fig. 10 is modelled by a dynamic droop-based inertial control including a deadband. When frequency deviation is larger than the deadband, G1 DFIGs start to release the power to support the frequency until their rotor speed is lower than 0.7 pu. Then, the Block I is disabled and rotor speed of G1 DFIGs starts to recover until their power output returns to MPPT output at optimum rotor speed. If rotor speed decreases below 0.7 pu., then a trip signal with a delay of 200 ms is sent to Block II. Therefore, a reserved power P_{boost} is released by G2 DFIGs until the corresponding optimum rotor speed is reached. The occurrence of SFD can be caused by a sudden loss of P_{droop} temporary power support from DFIGs. However, the amplitude of SFD is determined by the power P_{boost} reserved in the deloading DFIGs and the power shortage for the G1 DFIGs restoring the rotor speed. In addition, the duration for P_{boost} of the deloading DFIGs depends on the restoration phase of the G1 DFIGs.

5. Case study

In this section, simulations are done to evaluate the performance of the proposed consecutive dispatch of temporary and persistent energy reserves under varying wind speeds, power outputs and sizes of the tripping generator (SG2 shown in Fig. 8). To do this, wind speeds are varied from 8.5 m/s to 10 m/s with an increment of 0.5 m/s, sizes of the tripped generator are varied from 60 MW to 80 MW in increments of 10 MW and penetration level of wind power changes from 13 % to 25 %. The wake effect is neglected in the simulation.

As shown in Table 1, the proposed strategy is compared to Scheme 2 which applies the same dynamic droop as in proposed scheme to the entire DFIGs within a WF. In addition, it is compared to a case of a WF without inertial control through the time-domain simulations.

5.1. Effect of wind speeds

The performance of proposed scheme is affected by the wind speed, which contributes the various level of the WF KE over the frequency support period in a WF. This subsection examines the performance of the proposed scheme for cases that have wind speeds of 8.5 m/s and 9 m/s, respectively.

Case 1: Wind Speed of 8.5 m/s, 50 MW Generator Trip, Wind Power Penetration Level of 13 %: Fig. 11 shows the results for Case 1, in which SG2 is generating 50 MW prior to a disturbance in the system model and tripped at 10 s. As shown in Fig. 11(a), the first FNs for proposed scheme, Scheme 2 and Scheme 3 are 49.09 Hz, 49.13 Hz and 48.97 Hz respectively. Moreover, the SFDs for Scheme 1 and Scheme 2 are 49.18 Hz and 49.07 Hz, respectively.

Proposed scheme prevents the ω_r of G1 DFIGs from reaching $\omega_{\min}$. This is achieved by increasing the $R(df/dt)$ thus temporally decreasing P_{droop} at 16.7 s, as shown in Fig. 11(b). However, at the beginning stage of the contingency, ω_{r_de} of G2 DFIGs stays at a deloading level, and DFIGs in G2 contribute a deloaded level of power to the grid until the trip signal is received. Then ω_{r_de} starts to decrease to optimum rotor speed ω^* when P_{boost} of DFIGs in G2 is released to compensate the SFD. In contrast, in the Scheme 2 an SFD happens at 21.4 s when the WF output starts decreasing. A larger SFD occurs due to a bigger sudden loss of 12 MW temporary power than it does in the proposed scheme.

Table 1
Simulation schemes.

Schemes	Wind Turbines
1	Proposed scheme
2	Dynamic droop scheme
3	Without inertial control

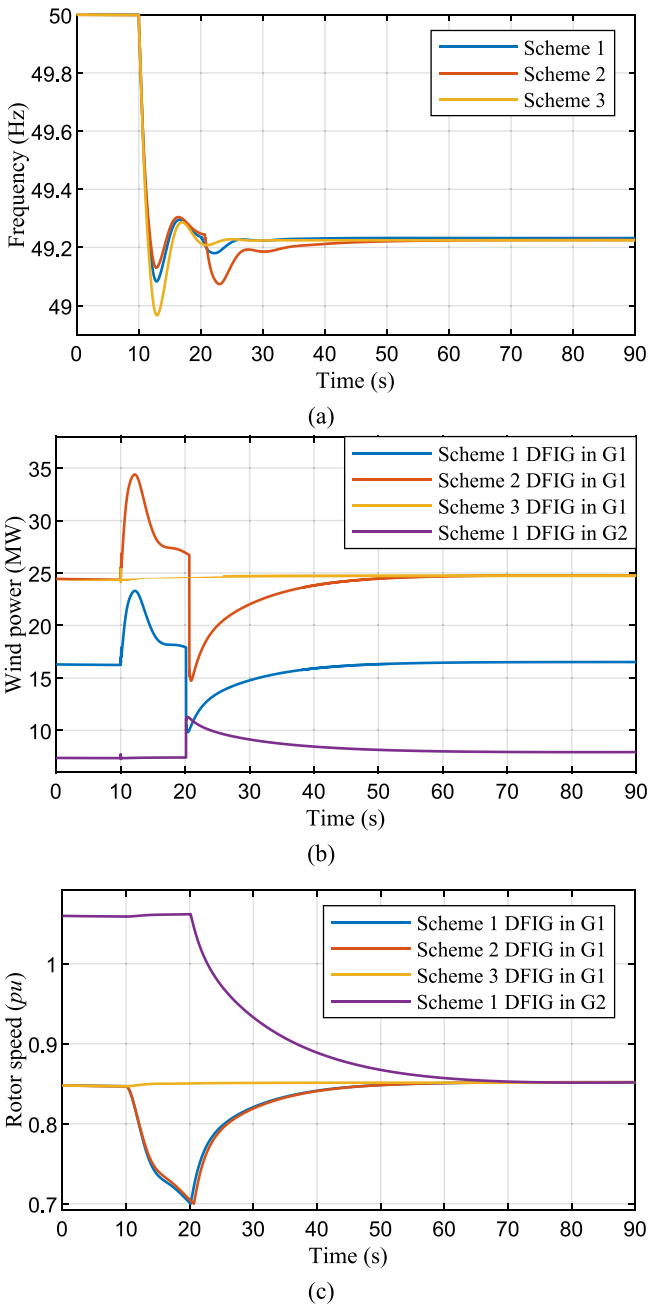

Fig. 11. Results for Case 1. (a) System frequency, (b) WF output, (c) Rotor speed.

Case 2: Wind Speed of 9 m/s, 50 MW Generator Trip, Wind Power Penetration Level of 13 %: Fig. 12 shows the results for Case 2, in which the wind speed is bigger than it is in Case 1. Therefore, KE of DFIGs is larger. As shown in Fig. 12(a), the first FNs for proposed scheme, Scheme 2 and Scheme 3 are 49.10 Hz, 49.13 Hz and 48.99 Hz respectively. In addition, the SFD for proposed scheme is 49.16 Hz, which is 0.06 Hz smaller than the first FN. Moreover, the SFD for Scheme 2 is 49.02 Hz. As in Case 2, proposed scheme has the smallest SFD among these two schemes, which is identical to Case 1.

The results of the above two cases prove that the proposed scheme

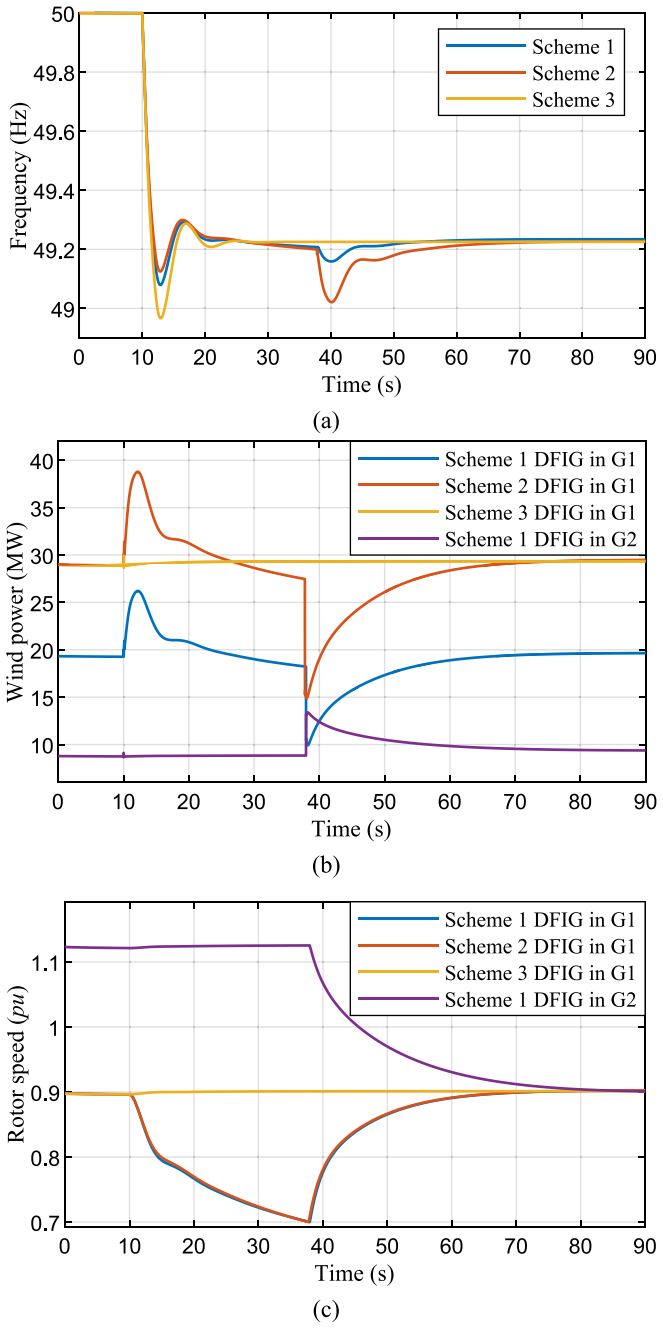

Fig. 12. Results for Case 2. (a) System frequency, (b) WF output, (c) Rotor speed.

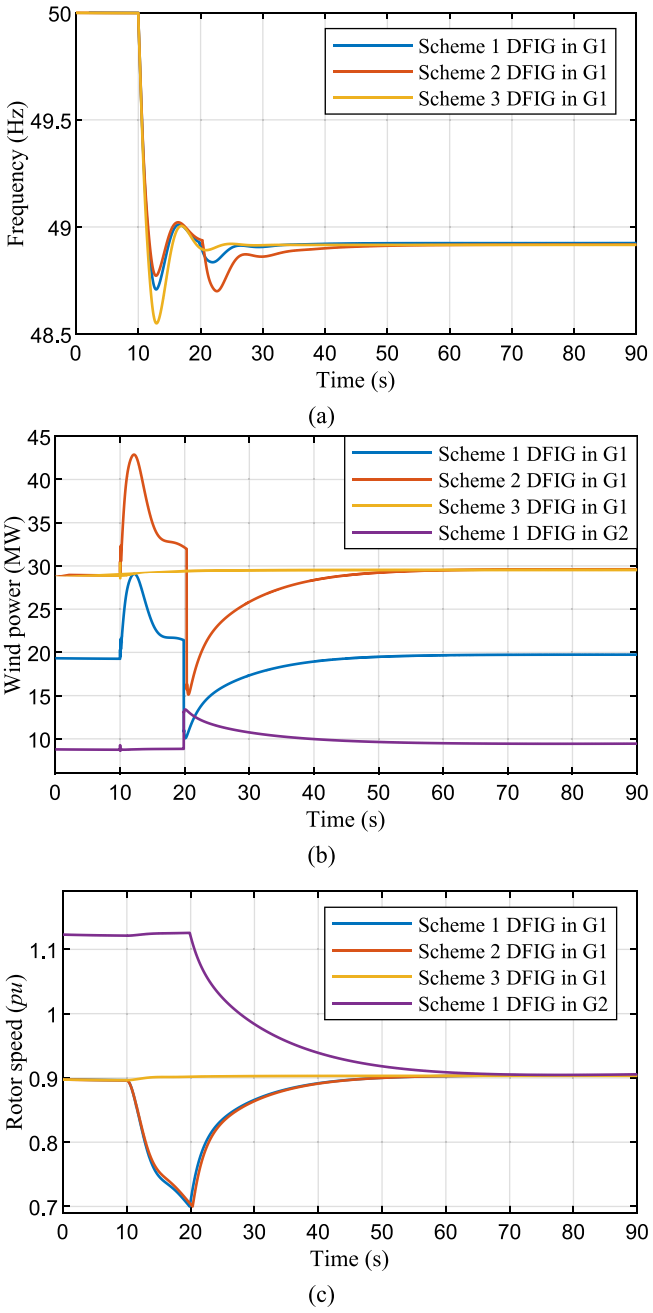

Fig. 13. Results for Case 3. (a) System frequency, (b) WF output, (c) Rotor speed.

can cause a smaller SFD while improving the FN in various wind speeds. However, in Case 2, ω_r recovering to ω^* takes longer period of time than it does in Case 1. Because both cases are set at same value of dynamic droop, DFIG having larger KE needs longer time to reach $\omega_{\min}$.

5.2. Effect of sizes of tripped generator

This subsection describes the results of applying the proposed scheme for different sizes of the tripped generator.

Case 3: Wind Speed of 9 m/s, 70 MW Generator Trip, Wind Power Penetration Level of 13 %: Fig. 13 shows the results for Case 3. The only exception is the size of the tripped generator. Also, the wind speed is the same as in Case 2, which means the same amount of KE can be generated by DFIGs. A generator delivering 70 MW to the netwrok is tripped at the moment of 10 s. This results in a larger frequency drop than in Case 2. The first FNs for proposed scheme, Scheme 2 and Scheme 3 are 48.71 Hz, 48.77 Hz, 48.55 Hz, respectively. An SFD for proposed scheme is 48.84 Hz, which is higher than the Scheme 2 by 0.14 Hz and is lower than that of Case 2 by 0.32 Hz.

It is worth noting that in this case, the size of tripped generator is greater than that of Case 2; thus, more power in Case 3 is released to stop frequency to decline than it does in Case 2. Additionally, the rotor speed of DFIGs decreases faster at the very first instants after the disturbance than in Case 2. However, frequency still recovers to the ω^* within the simulation time.

The results for Case 2 and Case 3 demonstrate that proposed scheme provides more temporary energy to improve SFD than Scheme 2, even when there is a larger frequency drop due to the larger size of tripped generator comes out.

5.3. Effects of wind power penetration levels

This subsection investigates the results of applications of the proposed scheme for different wind power penetration levels. To do this, the number of DFIGs is increased, whereas the capacity of SGs is reduced. The comparison is carried out by simulating two wind power penetration levels of 13 % and 25 %, respectively.

Case 4: Wind Speed of 9 m/s, 70 MW Generator Trip, Wind Power Penetration Level of 25 %: Fig. 14 shows the results for Cases 4. The simulation settings are identical to Case 5 except for wind penetration level of 25 %. The first FNs for proposed scheme, Scheme 2 and Scheme 3 are 48.83 Hz, 48.92 Hz and 48.55 Hz, repectively. In addition, the SFD for proposed scheme is 48.78 Hz, whereas Scheme 2 has an SFD of 48.5 Hz occuring at 33.9 s.

Comparing Fig. 13(a) with Fig. 14(a), the SFD becomes more severeunder higher wind power penetration level. The SFD of the Case 4 is 0.06 Hz larger than that of Case 3. Also, ω_r in the proposed scheme starts the recovery from 20.88 s and returns to its ω^*. Comparing to the Case 3, the time for recovery of ω_r is longer to ensure an adequate frequency response in Case 4.

6. Conclusion

In this paper, a consecutive power dispatch scheme for DFIG-based WFs is proposed. The scheme aims to mitigate SFDs and effectively restore rotor speed when DFIGs support the system frequency.

To address SFDs resulting from the withdrawal of temporary energy reserves in DFIGs, the proposed scheme coordinates temporary energy reserves with persistent energy reserves by categorizing all DFIGs within a WF into two groups. Group 1 (G1) DFIGs operate at MPPT curve, while the remaining DFIGs in Group 2 (G2) operate at a deloaded power level. During the initial stage of a disturbance, G1 DFIGs initiate frequency support using dynamic-droop based control. A trip signal is then transmitted to G2 DFIGs when the rotor speed of G1 DFIGs reaches its minimum limit. Consequently, the adverse effects of SFD are mitigated through additional boost power from G2 DFIGs.

Simulation results demonstrate that our proposed scheme effectively reduces the magnitude of SFD, enhances the FN, and prevents rotor overdecelerations. Moreover, it ensures the stable operation of DFIGs under various wind conditions, contingency sizes, and wind penetration levels. Additionally, the proposed scheme increases annual revenue when compared to WFs employing deloading control for all WTGs.

In the future work, it is essential to further investigate the optimal allocation of DFIGs in each group, taking into account factors such as wind speed and penetration level. This analysis will enable us to strike a balance between achieving optimal frequency control and maximizing annual revenue.

CRediT authorship contribution statement

Yi Cheng: Conceptualization, Formal analysis, Methodology, Software, Writing – original draft, Writing – review & editing. **Huadong Sun:** Supervision, Writing – review & editing. **Yuyuan Zhang:** Writing – original draft, Writing – review & editing. **Shiyun Xu:** Software, Validation. **Bing Zhao:** Supervision, Validation. **Petr Vorobev:** Validation, Writing – review & editing. **Vladimir Terzija:** Supervision, Writing – review & editing.

Declaration of competing interest

The authors declare that they have no known competing financial interests or personal relationships that could have appeared to influence the work reported in this paper.

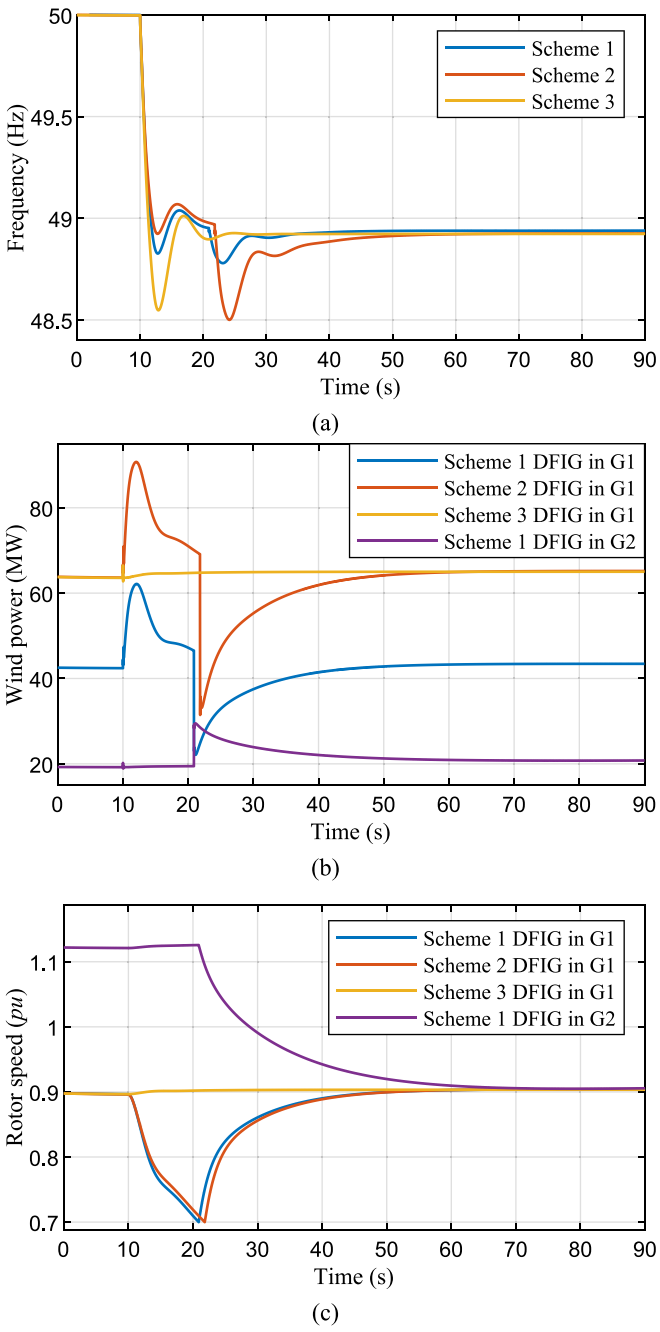

Fig. 14. Results for Case 4. (a) System frequency, (b) WF output, (c) Rotor speed.

Data availability

Data will be made available on request.

Acknowledgements

This paper was supported in part by National Natural Science Foundation of China under Grant U2166601.

References

[1] IRENA. Future of wind: Deployment, investment, technology, grid integration and socio-economic aspects (A Global Energy Transformation paper). International Renewable Energy Agency, Abu Dhabi; 2019.
[2] Kroposki B, Johnson B, Zhang Y, Gevorgian V, Denholm P, Hodge B-M, et al. Achieving a 100% renewable grid: operating electric power systems with extremely

high levels of variable renewable energy. IEEE Power Energy Mag 2017;15:61–73. https://doi.org/10.1109/MPE.2016.2637122.
[3] Technical Requirements for the Connection of Generation Facilities to the Hydro-Québec Transmission System. Montreal, QC, Canada: Hydro Québec; 2009.
[4] De Almeida RG, Castronuovo ED, Lopes JP. Optimum generation control in wind parks when carrying out system operator requests. IEEE Trans Power Syst 2006;21:718–25. https://doi.org/10.1109/TPWRS.2005.861996.
[5] Chen Z, Shi T, Song P, Li C, Cao Y, Yan Y. Improved pitch control strategy for the robust operation of wind energy conversion system in the high wind speed condition. Int J Electr Power Energy Syst 2023;153:109381. https://doi.org/10.1016/j.ijepes.2023.109381.
[6] Vidyanandan KV, Senroy N. Primary frequency regulation by deloaded wind turbines using variable droop. IEEE Trans Power Syst 2013;28:837–46. https://doi.org/10.1109/TPWRS.2012.2208233.
[7] Luo H, Hu Z, Zhang H, Chen H. Coordinated active power control strategy for deloaded wind turbines to improve regulation performance in AGC. IEEE Trans Power Syst 2019;34:98–108. https://doi.org/10.1109/TPWRS.2018.2867232.
[8] Mahvash H, Taher SA, Rahimi M, Shahidehpour M. Enhancement of DFIG performance at high wind speed using fractional order PI controller in pitch compensation loop. Int J Electr Power Energy Syst 2019;104:259–68.
[9] Hwang M, Muljadi E, Jang G, Kang YC. Disturbance-adaptive short-term frequency support of a DFIG associated with the variable gain based on the ROCOF and rotor speed. IEEE Trans Power Syst 2017;32:1873–81. https://doi.org/10.1109/TPWRS.2016.2592535.
[10] Hwang M, Muljadi E, Park J-W, Sorensen P, Kang YC. Dynamic droop-based inertial control of a doubly-fed induction generator. IEEE Trans Sustain Energy 2016;7:924–33. https://doi.org/10.1109/TSTE.2015.2508792.
[11] Guo Y, Bao W, Ding L, Liu Z, Kheshti M, Wu Q, et al. Analytically derived fixed termination time for stepwise inertial control of wind turbines—Part II: application strategy. Int J Electr Power Energy Syst 2020;121:106106. https://doi.org/10.1016/j.ijepes.2020.106106.
[12] Yang D, Wang X, Yan G-G, Jin E, Huang J, Zheng T, et al. Decoupling active power control scheme of doubly-fed induction generator for providing virtual inertial response. Int J Electr Power Energy Syst 2023;149:109051. https://doi.org/10.1016/j.ijepes.2023.109051.
[13] Ouyang J, Pang M, Li M, Zheng D, Tang T, Wang W. Frequency control method based on the dynamic deloading of DFIGs for power systems with high-proportion wind energy. Int J Electr Power Energy Syst 2021;128:106764. https://doi.org/10.1016/j.ijepes.2021.106764.
[14] Liu Z, Ding L, Wang K, Ma Z, Bao W, Liu Q. Control strategy to mitigate secondary frequency dips for DFIG with virtual inertial control. In: 2016 China International Conference on Electricity Distribution (CICED). IEEE; 2016. p. 1–5. https://doi.org/10.1109/CICED.2016.7576211.
[15] Yang D, Kim J, Kang YC, Muljadi E, Zhang N, Hong J, et al. Temporary frequency support of a DFIG for high wind power penetration. IEEE Trans Power Syst 2018;33:3428–37. https://doi.org/10.1109/TPWRS.2018.2810841.
[16] Yang D, Yan G-G, Zheng T, Zhang X, Hua L. Fast frequency response of a DFIG based on variable power point tracking control. IEEE Trans Ind Appl 2022;58:5127–35. https://doi.org/10.1109/TIA.2022.3177590.
[17] Conroy JF, Watson R. Frequency response capability of full converter wind turbine generators in comparison to conventional generation. IEEE Trans Power Syst 2008;23:649–56. https://doi.org/10.1109/TPWRS.2008.920197.
[18] De Paola A, Angeli D, Strbac G. Scheduling of wind farms for optimal frequency response and energy recovery. IEEE Trans Control Syst Technol 2016;24:1764–78. https://doi.org/10.1109/TCST.2016.2514839.
[19] El Itani S, Annakkage UD, Joos G. Short-term frequency support utilizing inertial response of DFIG wind turbines. In: 2011 IEEE Power and Energy Society General Meeting. IEEE; 2011. p. 1–8. https://doi.org/10.1109/PES.2011.6038914.
[20] Söder L, Ackermann T. Wind Power in Power Systems. 2012.
[21] Shen P, Guan L, Huang Z, Wu L, Jiang Z. Active-current control of large-scale wind turbines for power system transient stability improvement based on perturbation estimation approach. Energies 2018;11:1995. https://doi.org/10.3390/en11081995.
[22] Lee J, Muljadi E, Srensen P, Kang YC. Releasable kinetic energy-based inertial control of a DFIG wind power plant. IEEE Trans Sustain Energy 2016;7:279–88. https://doi.org/10.1109/TSTE.2015.2493165.
[23] Geng H, Xu D, Wu B, Yang G. Active damping for PMSG-based WECS with DC-link current estimation. IEEE Trans Ind Electron 2011;58:1110–9. https://doi.org/10.1109/TIE.2010.2040568.
[24] Jain P, Wijayatunga P. Grid Integration of Wind Power: Best Practices for Emerging Wind Markets n.d.
[25] Kennedy JM, Fox B, Littler T, Flynn D. Validation of fixed speed induction generator models for inertial response using wind farm measurements. IEEE Trans Power Syst 2011;26:1454–61. https://doi.org/10.1109/TPWRS.2010.2081385.
[26] Chen Z, Guerrero JM, Blaabjerg F, Member S. A review of the state of the art of power electronics for wind turbines. IEEE Trans Power Electron 2009;24:1859–75. https://doi.org/10.1109/TPEL.2009.2017082.
[27] Morren J, de Haan SWH, Kling WL, Ferreira JA. Wind turbines emulating inertia and supporting primary frequency control. IEEE Trans Power Syst 2006;21:433–4. https://doi.org/10.1109/TPWRS.2005.861956.
[28] Janssens NA, Lambin G, Bragard N. Active power control strategies of DFIG wind turbines. IEEE Lausanne Power Tech 2007;2007:516–21. https://doi.org/10.1109/PCT.2007.4538370.
[29] Madsen J, Findrik M, Madsen T, Schwefel H-P. Optimizing data access for wind farm control over hierarchical communication networks. Int J Distrib Sens Netw 2016;2016:1–14. https://doi.org/10.1155/2016/5936235.